Journal of Organometallic Chemistry, 472 (1994) 317–328

Investigation of $[(py)(Et)Co(dmg \cdot GaEt_2)_2]$ and $[Ni(dmg \cdot GaEt_2)_2]$ (py = pyridine; dmg = dimethylglyoximato) as single source precursors for deposition of β-CoGa and NiGa by MOCVD. Crystal structure of $[(py)(Et)Co(dmg \cdot GaEt_2)(dmgH)]$ *

B. Fraser, L. Brandt, W.K. Stovall, H.D. Kaesz and S.I. Khan

Department of Chemistry and Biochemistry, University of California, Los Angeles, CA 90024-1569 (USA)

F. Maury

CNRS-URA 445, Ecole Nationale Supérieure de Chimie, 31077 Toulouse cédex (France)

(Received October 26, 1993; in revised form January 18, 1994)

Abstract

The complexes $[(py)(Et)Co(dmg \cdot GaEt_2)_2]$, **1**, and $[Ni(dmg \cdot GaEt_2)_2]$, **2**, (dmg = dimethylglyoxime) were synthesized for study as potential precursors for Metalorganic Chemical Vapor Deposition (MOCVD) of β-CoGa and NiGa. Complex **1** is easily hydrolyzed to $[(py)(Et)Co(dmgH)(dmg \cdot GaEt_2)]$, **3**; a single crystal X-ray structure was obtained for this product.

Thermogravimetric analyses (TGA) under H_2 flow resulted in a residual mass of 35% at 650°C for **1** (residual for $CoGa_2$ is 31%) and 29% at 500°C for **2** (residual for $NiGa_2$ is 36%). The highest peaks in the electron impact MS corresponded to $(MWt - py - 2C_2H_5)^+$, **1**, and $(MWt - C_2H_5)^+$, **2**. The next peaks for both compounds corresponded to loss of the remaining ethyl groups.

MOCVD at 560°C resulted in polycrystalline β-CoGa (using **1** as a precursor) and polycrystalline NiGa (**2**). Upon raising the temperature of the GaAs substrate to 630°C, **1** gave films with areas of epitaxial growth in a primarily polycrystalline β-CoGa film; partial degradation of the substrate also occurs. EDS and XPS data showed how film composition can be controlled by precursor design. EDS analysis of the CoGa (1:2.4) and NiGa (1:2.0) films showed that stoichiometry of the precursors was principally retained. The films exhibit only negligible carbon or nitrogen contamination, but the oxygen content is relatively high (10–20%). XPS data show that oxygen near the surface is bonded to both Co and Ga, but in the film, oxygen is only bonded to Ga.

Key words: MOCVD; Cobalt-gallium; Nickel-gallium; Epitaxial growth; Dimethylglyoximato

1. Introduction

Fabrication of III–V semiconductor devices is limited by the lack of epitaxial and thermodynamically stable metal/semiconductor interfaces. The transition metal gallides and aluminides are conductors which can fulfill this need [1]. Metalorganic Chemical Vapor Deposition (MOCVD) using single source precursors offers among other advantages a control of stoichiometry [2]; for systems with complicated phase diagrams, multiple phase deposits usually result unless stoichiometry is controlled [3].

Control of stoichiometry from the single source precursor $(CO)_4CoGaCl_2(THF)$ was earlier demonstrated [4,5]; polycrystalline β-$Co_{0.5}Ga_{0.5}$ films were obtained. This metallic conductor however, is not lattice matched to (100)GaAs until the Ga content reaches 63%, or a Ga:Co ratio of approximately 2:1. Epitaxial growth of β-$Co_{0.37}Ga_{0.63}$ on (100)GaAs has now been achieved by MOCVD using the separate sources $(\eta^5\text{-}C_5H_5)Co(CO)_2$ and Et_3Ga [6]. We were thus interested to discover if this could also be achieved using a single source precursor containing a Co:Ga ratio of 1:2. Previously we have reported that thin polycrystalline

Correspondence to: Professor H.D. Kaesz.

* Dedicated to Professor Helmut Werner on the occasion of his 60th birthday.

SSDI 0022-328X(94)24506-E

Elsevier Sequoia.

films of $PtGa_2$ can be obtained by short path MOCVD using the substituted glyoximato complex [Pt(dmg · $GaMe_2)_2$] [4]. The analogous complexes [M(dmg · $GaMe_2)_2$] (M = Ni, Pd, Pt, Cu) have been described in the literature [7]. However, we proceeded to synthesize the ethyl derivative, [(py)(Et)Co(dmg · $GaEt_2)_2$], **1**, in order to reduce the chance of carbon contamination in MOCVD studies [8]. Additionally, we have synthesized [Ni(dmg · $GaEt_2)_2$], **2**, [7] and describe its deposition behavior.

2. Experimental details

2.1. General

All syntheses were performed using Schlenk techniques or in a Vacuum Atmosphere argon filled dry box. Pentane was distilled over CaH_2 under At atmosphere. $GaEt_3$ was purchased from Strem Chemicals, Inc. [Co(Me)(dmg)py] [9] and [Ni(dmg)$_2$] [10] have been prepared according to literature procedures. Their ^{1}H- and ^{13}C-NMR data which were not reported earlier were as follows:

[Co(Me)(dmg)py]: ^{1}H-NMR (200.133 MHz, 23°C, CD_2Cl_2) δ(ppm) 0.67 (s, Co-CH_3, 3H), 2.08 (s, CH_3, 12H), 7.3–7.4 (m, Co-py, 2H), 7.7–7.8 (m, Co-py, 1H), 8.5–8.6 (m, Co-py, 2H), 13.67 (br.s, OH of dmg, 2H). ^{13}C-NMR (50.323 MHz, 23°C, CD_2Cl_2) δ(ppm) 12.24 (CH_3 of dmg), 125.73, 138.07, 150.47 (Co-py), 149.54 (Cq of dmg); Co-CH_3 not resolved.

[Ni(dmg)$_2$]: ^{1}H-NMR (200.133 MHz, 23°C, CD_2Cl_2) δ(ppm) 0.23 (s, CH_3, 12H); OH of dmg not resolved.

^{1}H- and ^{13}C-NMR spectra were recorded on a Bruker spectrometer at 200.133 and 50.323 MHz respectively. Spectra were referenced using the residual protons or carbons of C_6D_6 at 7.15 ppm or 128 ppm, or CD_2Cl_2 at 5.32 ppm or 54.0 ppm. Elemental analyses were performed by Desert Analytics.

2.1.1. Synthesis of [(py)(Et)Co(dmg · $GaEt_2)_2$], 1

A solution of 1.0 g (2.6 mmol) [(py)(Me)Co(dmg)$_2$] suspended in 20 ml of pentane was magnetically stirred under argon. A solution of 1.0 ml (6.3 mmol) $GaEt_3$ in 10 ml of pentane was added over a period of 20 min. After a total reaction time of 4 h, volatile components were removed *in vacuo*. The crude orange-brown residue was recrystallized from 8 ml of pentane at −20°C. The supernatant liquid was removed and the solid washed with cold pentane. Evaporation to dryness yielded 1.1 g (65%) orange, slightly air sensitive microcrystals of **1**. Compound **1** was soluble in aliphatic and aromatic solvents and melted at 85°C under decomposition.

Anal. calc. for $C_{23}H_{42}O_4N_5Ga_2Co$: 42.43% C, 6.52% H, 10.76% N; found 40.52% C, 6.41% H, 10.53% N. ^{1}H-NMR (200.133 MHz, 23°C, C_6D_6) δ(ppm) 0.52 (t, Co-CH_2-CH_3, 3H; $J(^1H-^1H) = 7.5$ Hz), 0.86 (q, Ga-CH_2-CH_3, 4H; $J(^1H-^1H) = 8.1$ Hz), 1.03 (q, Ga-CH_2-CH_3, 4H; $J(^1H-^1H) = 8.0$ Hz), 1.48 (t, Ga-CH_2-CH_3, 6H; $J(^1H-^1H) = 8.1$ Hz), 1.71 (t, Ga-CH_2-CH_3, 6H; $J(^1H-^1H) = 7.9$ Hz), 1.72 (s, CH_3, 12H), 2.99 (q, Co-CH_2-CH_3, 2H; $J(^1H-^1H) = 7.5$ Hz), 6.6–6.7 (m, Co-py, 3H), 9.1–9.2 (m, Co-py, 2H). ^{13}C-NMR (50.323 MHz, 23°C, C_6D_6) δ(ppm) 3.49 (Ga-CH_2-CH_3), 5.99 (Ga-CH_2-CH_3), 10.28 (Ga-CH_2-CH_3), 10.49 (Ga-CH_2-CH_3), 12.62 (CH_3 of dmg), 16.34 (Co-CH_2-CH_3), 19.1 (br, tentatively assigned to Co-CH_2), 124.54, 137.20, 151.13 (Co-py) 154.12 (C_q of dmg).

2.1.2. Synthesis of [Ni(dmg · $GaEt_2)_2$], 2

A solution of 1.0 g (3.5 mmol) [Ni(dmg)$_2$] suspended in 20 ml of pentane was magnetically stirred under argon and slowly allowed to react with a solution of 1.1 ml (7.3 mmol) $GaEt_3$ in 10 ml of pentane. After a total reaction time of 4 h, volatile components were removed *in vacuo*. The crude red-brown residue was recrystallized from 8 ml of pentane at −20°C. The supernatant liquid was removed and the solid washed with cold pentane. Evaporation to dryness yielded 1.3 g (70%) red, slightly air sensitive microcrystals of **2**. Compound **2** was soluble in aliphatic and aromatic solvents and melted at 105°C under decomposition.

Anal. calc. for $C_{16}H_{32}O_4N_4Ga_2Ni$: 35.41% C, 5.96% H, 10.33% Co; found 35.16% C, 6.02% H, 10.14% Co. ^{1}H-NMR (200.133 MHz, 23°C, C_6D_6) δ(ppm) 0.98 (q, Ga-CH_2-CH_3, 8H; $J(^1H-^1H) = 8.1$ Hz), 1.51 (t, Ga-CH_2-CH_3, 12H; $J(^1H-^1H) = 8.1$ Hz), 1.70 (s, CH_3, 12H). ^{13}C-NMR (50.323 MHz, 23°C, C_6D_6) δ(ppm) 3.35 (Ga-CH_2-CH_3), 10.27 (CH_3 of dmg), 12.52 (Ga-CH_2-CH_3), 157.47 (C_q of dmg).

2.1.3. Synthesis of [(py)(Et)Co(dmgH)(dmg · $GaEt_2$)], 3

In an attempted crystallization, a solution of 50 mg of **1** in 2 ml pentane was allowed to stand in air for a period of four days covered with a watch glass. Dark orange crystals were obtained. The supernatant liquid was decanted and the residue washed with 2 ml of pentane. After drying in an argon stream 0.64 g of the air-stable product was obtained (80%) yield). The crystals proved to be the hydrolysis product **3** by single crystal X-ray diffraction (see below). Apparently, the gradual diffusion of moisture caused hydrolysis of one of the two $GaEt_2$ groups in **1**; this product was much less soluble than **1** in pentane and precipitates from the solution. Compound **3** was soluble in aromatic solvents.

^{1}H-NMR (200.133 MHz, 23°C, C_6D_6) δ(ppm) 0.74 (t, Co-CH_2-CH_3), 3H; $J(^1H-^1H) = 7.6$ Hz), 0.90 (q,

Ga-CH_2-CH_3, 2H; $J(^1H-^1H) = 8.1$ Hz), 1.02 (q, Ga-CH_2-CH_3, 2H; $J(^1H-^1H) = 8.0$ Hz), 1.51 (t, Ga-CH_2-CH_3, 3H; $J(^1H-^1H) = 8.1$ Hz), 1.77 (t, Ga-CH_2-CH_3, 6H; $J(^1H-^1H) = 8.0$ Hz), 1.73 (s, CH_3, 6H), 1.80 (s, CH_3, 6H), 2.56 (q, Co-CH_2-CH_3, 2H; $J(^1H-^1H) = 7.7$ Hz), 6.5–6.7 (m, Co-py, 3H), 9.0–9.1 (m, Co-py, 2H), 11.83 (br. s, OH of dmg, 1H). ^{13}C-NMR (50.323 MHz, 23°C, C_6D_6) δ(ppm) 4.15 (Ga-CH_2-CH_3), 6.82 (Ga-CH_2-CH_3), 10.32 (Ga-CH_2-CH_3), 10.61 (Ga-CH_2-CH_3), 12.00 (CH_3 of dmg), 12.08 (CH_3 of dmg), 16.54 (Co-CH_2-CH_3), 124.63, 137.06, 150.75 (Co-py), 148.90, 154.00 (C_q of dmg); Co-CH_2 not found.

2.2. X-ray data collection and refinement

A crystal of **3** of approximate dimension 0.25 × 0.20 × 0.05 mm sealed in a glass capillary was mounted on a modified Picker four-circle automated diffractometer equipped with a gas-stream low-temperature device, scintillation counter, and a graphite monochromatized Mo Kα source. Accurate unit cell parameters are given in Table 1 along with other experimental details. A full table of data collection and structure refinement parameters is given as Supplementary Table A. The unit cell parameters and orientation matrix were obtained by a least-squares fit to the automatically centered settings of 37 reflections. One quadrant of diffraction data ($+h$, $+k$, $\pm l$) were collected with a θ–2θ scan mode up to a maximum 2θ of 55°. The intensities of three standard reflections were recorded after every 97 reflections collected and showed no significant variations throughout the data collection. A total of 5870 reflections were collected of which 2888 independent reflections with intensities greater than 3σ were retained for structure analysis. Intensities were derived from an analysis of scan profiles [11]. The data were corrected for Lorentz and polarization effects and a y-scan procedure was used for an empirical absorption correction.

TABLE 1. Crystal data for [(py)(Et)Co(dmg·$GaEt_2$)(dmgH)] **3**

Formula	$CoGaN_5O_4C_{19}H_{33}$
F.W.	524.15
Cryst. syst.	monoclinic
Space group	$P2_1/a$ (no. 14)
Cryst. dimens., mm	0.25×0.20×0.05
Cryst. color	orange yellow
Cryst. habit	platelet
a, Å	17.366(1)
b, Å	8.350(1)
c, Å	16.211(1)
β, °	98.96(1)
z	4
V, Å^3	2321.9(3)
ρ(calcd), g cm^{-3}	1.50
Radiation, λ	Mo Kα 0.7107
Abs. coeff. (μ), cm^{-1}	30.45
Abs. factor range (Intensity)	1.19 to 1.00
F(000), e	1088
Temp., K	156
Diffractometer	Picker (Crystal Logic)
Scan mode, speed (° min^{-1})	θ–2θ, 7.5
2θ range, °	1–55
Total data collcd., unique data used	5870, 2888 ($I > 3\sigma(I)$)
No. or parms. refined	281
Final shift/error, max. and avg.	0.023, 0.002
Max resid. density, e Å^{-3}	1.10
$R = \Sigma w \|\|F_o\| - \|F_c\|\| / \Sigma \|F_o\|$	0.047
$R_w = [\Sigma w(\|F_o\| - \|F_c\|)^2 / \Sigma w \|F_o\|^2]^{1/2}$	0.052
GOF = $[\Sigma(w\|\|F_o\| - \|F_c\|\|)^2/(N_o - N_p)]^{1/2}$	1.293

The structure was solved in the monoclinic space group $P2_1/a$ (no. 14) by direct methods of SHELX86, which revealed the positions of all non-hydrogen atoms. This was followed by several cycles of full-matrix least-squares refinement. Hydrogen atoms were included as fixed contributors to the final refinement cycles. The positions of hydrogen atoms were calculated on the basis of idealized geometry and bond length (C–H = 1.00 Å), and were assigned isotropic temperature factors 30% greater than the other atoms in the structure. For methyl groups, at least one of the hydrogen atom positions was located from a difference electron density map.

One of the methyl carbon atoms, C(19), was disordered and refined at two positions with occupancy factors of 60 and 40 percent, respectively. In the final cycles of least-squares refinement, all non-hydrogen atoms were refined with anisotropic thermal coefficients. Convergence results in final agreement factors shown in Table 1. An ORTEP projection is shown in Fig. 1. The final atomic positional parameters are given in Table 2; selected interatomic distances and angles are given in Table 3. Derived positional parameters for the hydrogen atoms and anisotropic thermal parameters are given in Supplementary Tables B and C, respectively.

2.3. Substrate pretreatment and MOCVD apparatus

Disks of (100)GaAs (7 cm dia.) were purchased from Laser Diode, Inc. (Metuchen, NJ); disks of (100)Si (10 cm dia.) were purchased from Atomergic Chemetals Corporation (Farmingdale, NY). Small squares (1 × 1 cm) were cut from the disks and degreased first in hot trichloroethylene and then in acetone at room temperature. The substrates were etched to remove surface damage: the GaAs was treated in a solution of H_2SO_4:H_2O_2:H_2O (5:1:1 by volume) while the Si was immersed in 20% aqueous HF. The substrates were then each rinsed with distilled H_2O and dried under argon.

Experiments were performed in an isothermal (hot wall) CVD reactor shown in Fig. 2. H_2 gas was purified by passing through an oxygen absorbent catalyst (oxysorb 20–60 mesh; 200°C) and molecular sieves (4 Å; liquid N_2). The precursors were ground under nitrogen in an inert amosphere chamber. The powder was then transferred through a long necked glass funnel to the sample compartment in the reactor which is held vertically in the dry box. The reactor is then turned to a horizontal position and the pre-treated substrates are put into place. The reactor is stoppered and transferred to its position in the MOCVD apparatus. This is flushed with purified hydrogen and evacuated for 1 h. Typical growth conditions are summarized in Table 4. During the deposition, precursor and substrate were heated by heating tapes. A trap was placed at the outlet of the reactor in order to collect the condensible products at liquid nitrogen temperature.

2.4. General instrumentation for screening of precursors and for characterization of thin films

The mass spectra of **1** and **2** have been recorded under electronic impact using an ionization energy = 70 eV (source temperature 120°C). Thermogravimetric analyses were performed using a Du Pont 5900 model with either H_2, Ar, or N_2 flow through the furnace. The film morphologies were analyzed by scanning electron microscopy (SEM). Surface composition was determined by X-ray photoelectron spectroscopy (XPS) and energy dispersive spectroscopy (EDS). Layer thickness was determined by SEM of the film cross section. Surface structure was analyzed by reflection high energy electron diffraction (RHEED) with bean energy of 30 KeV at a glancing angle of 1–2°. Immediately before analysis the samples were cleaned by dipping in dilute HCl and then rinsing with distilled water. Depth profiling was determined by secondary ion mass spectrometry (SIMS).

TABLE 2. Positional parameters for [(py)(Et)Co(dmg·$GaEt_2$)(dmgH)], **3**, with e.s.d.'s in parenthesis

Atom	x	y	z	$U_{eq} \times 10^3$ [a]
Co	0.6098(1)	0.0854(1)	0.7165(1)	17(1)
Ga	0.7682(1)	0.1579(1)	0.8896(1)	24(1)
N(1)	0.5820(3)	−0.0986(6)	0.6504(3)	21(3)
N(2)	0.7024(3)	−0.0417(6)	0.7490(3)	20(3)
N(3)	0.5159(3)	0.1988(6)	0.6837(3)	22(3)
N(4)	0.6331(3)	0.2756(5)	0.7826(3)	17(3)
N(5)	0.6605(2)	0.1879(5)	0.6221(3)	17(3)
O(1)	0.7680(2)	0.0020(5)	0.8002(2)	26(2)
O(2)	0.5122(2)	−0.1124(5)	0.5974(2)	29(3)
O(3)	0.7024(2)	0.3175(5)	0.8280(2)	25(2)
O(4)	0.4574(2)	0.1468(5)	0.6252(2)	28(2)
C(1)	0.6315(3)	−0.2148(7)	0.6544(3)	19(3)
C(2)	0.7024(3)	−0.1820(7)	0.7134(3)	22(3)
C(3)	0.7685(3)	−0.2975(8)	0.7305(4)	31(4)
C(4)	0.6170(4)	−0.3629(8)	0.6021(4)	30(4)
C(5)	0.5088(3)	0.3388(7)	0.7171(3)	22(3)
C(6)	0.5780(3)	0.3828(7)	0.7763(3)	21(3)
C(7)	0.4387(4)	0.4453(7)	0.6957(4)	30(4)
C(8)	0.5855(4)	0.5361(7)	0.8232(4)	30(4)
C(9)	0.7336(3)	0.2458(7)	0.6366(3)	22(3)
C(10)	0.7689(3)	0.3181(7)	0.5750(3)	24(3)
C(11)	0.7275(3)	0.3314(8)	0.4956(4)	27(4)
C(12)	0.6523(4)	0.2714(7)	0.4800(3)	27(4)
C(13)	0.6208(3)	0.1990(7)	0.5436(3)	23(3)
C(14)	0.5605(4)	−0.0143(7)	0.8103(3)	26(4)
C(15)	0.4785(4)	−0.0802(8)	0.7880(4)	36(4)
C(16)	0.7163(4)	0.0710(9)	0.9808(3)	35(4)
C(17)	0.6681(5)	0.191(1)	1.0199(5)	59(6)
C(18)	0.8731(4)	0.2494(9)	0.8958(4)	37(4)
C(19A)	0.935(1)	0.124(4)	0.935(2)	54(16)
C(19B)	0.9322(9)	0.225(3)	0.969(1)	59(12)

[a] $U_{eq} = [1/(6\pi^2)] \times \Sigma_i \Sigma_j \beta_{ij} (\boldsymbol{a}_i \cdot \boldsymbol{a}_j)$.

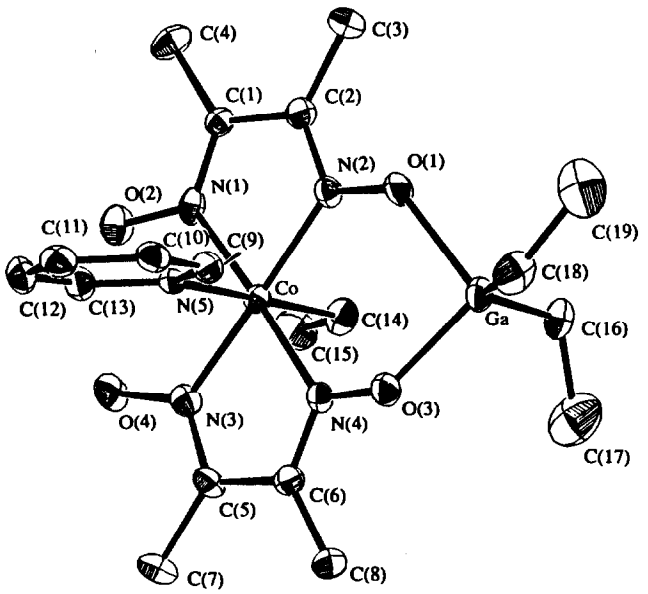

Fig. 1. ORTEP projection of for [(py)(Et)Co(dmg·$GaEt_2$)(dmgH)], **3**; the H atom bridging between O(2) and O(4) has not been located and is not shown.

3. Screening of the precursor

3.1. Mass spectrometry analysis

This technique was used to obtain insight about labile groups and a likely decomposition process. Peaks have been identified by the respective isotopic ratios.

While no peak for the parent molecular ion (m/e = 651) is observed in the MS of **1**, a high intensity peak was seen at m/e = 514 (100%). The latter corresponds to the loss of 2 ethyl groups and pyridine. The next two major peaks at m/e = 455 (30%) and 426 (20%) suggest loss of additional ethyl groups leaving the fragment Co(dmgGa)$_2$. Due to exceedingly branched de-

TABLE 3. Selected internuclear separations (°) and angles (°) for [(py)(Et)Co(dmg·$GaEt_2$)(dmgH)], **3**, with e.s.d.'s in parenthesis

Co–N(3)	1.889(5)	N(4)–C(6)	1.303(7)
Co–N(1)	1.892(5)	N(4)–O(3)	1.355(5)
Co–N(4)	1.923(4)	N(5)–C(9)	1.344(6)
Co–N(2)	1.930(5)	N(5)–C(13)	1.353(6)
Co–C(14)	2.036(6)	C(1)–C(2)	1.462(7)
Co–N(5)	2.066(4)	C(1)–C(4)	1.498(8)
		C(2)–C(3)	1.492(8)
Ga–O(3)	1.930(4)	C(5)–C(6)	1.463(7)
Ga–O(1)	1.948(4)	C(5)–C(7)	1.504(8)
		C(6)–C(8)	1.484(8)
Ga–C(18)	1.963(6)	C(9)–C(10)	1.389(8)
Ga–C(16)	1.985(6)	C(10)–C(11)	1.378(7)
		C(11)–C(12)	1.385(8)
N(1)–C(1)	1.291(7)	C(12)–C(13)	1.380(8)
N(1)–O(2)	1.377(5)	C(14)–C(15)	1.517(8)
N(2)–C(2)	1.306(7)	C(16)–C(17)	1.51(1)
N(2)–O(1)	1.351(5)	C(18)–C(19B)	1.46(2)
N(3)–C(5)	1.302(7)	C(18)–C(19A)	1.56(2)
N(3)–O(4)	1.349(5)	C(19A)–C(19B)	1.02(2)
N(3)–Co–N(1)	96.6(2)	N(2)–O(1)–Ga	122.8(3)
N(3)–Co–N(4)	80.8(2)	Ga–O(1)–C(2)	149.0(3)
N(3)–Co–N(2)	176.7(2)	N(4)–O(3)–Ga	120.5(3)
N(3)–Co–C(14)	88.3(2)	Ga–O(3)–C(6)	144.5(3)
N(3)–Co–N(5)	91.9(2)	N(1)–C(1)–C(2)	112.2(5)
N(1)–Co–N(4)	177.3(2)	N(1)–C(1)–C(4)	122.7(5)
N(1)–Co–N(2)	80.6(2)	C(2)–C(1)–C(4)	125.1(5)
N(1)–Co–C(14)	89.5(2)	C(2)–C(1)–O(2)	143.9(4)
N(1)–Co–N(5)	91.0(2)	C(4)–C(1)–O(2)	91.0(4)
N(4)–Co–N(2)	102.0(2)	N(2)–C(2)–C(1)	113.5(5)
N(4)–Co–C(14)	89.9(2)	N(2)–C(2)–C(3)	123.4(5)
N(4)–Co–N(5)	89.6(2)	N(2)–C(2)–N(1)	82.0(4)
N(2)–Co–C(14)	90.0(2)	C(1)–C(2)–C(3)	123.1(5)
N(2)–Co–N(5)	89.8(2)	C(1)–C(2)–O(1)	145.4(4)
C(14)–Co–N(5)	179.5(2)	C(3)–C(2)–O(1)	91.4(4)
O(3)–Ga–O(1)	98.3(2)	C(3)–C(2)–N(1)	154.6(4)
O(3)–Ga–C(18)	103.2(2)	O(1)–C(2)–N(1)	114.0(3)
O(3)–Ga–C(16)	109.7(2)	N(3)–C(5)–C(6)	112.1(5)
O(1)–Ga–C(18)	101.1(2)	N(3)–C(5)–C(7)	124.1(5)
O(1)–Ga–C(16)	111.2(2)	C(6)–C(5)–C(7)	123.7(5)
C(18)–Ga–C(16)	129.0(3)	C(6)–C(5)–O(4)	143.6(4)
C(1)–N(1)–O(2)	118.9(5)	C(7)–C(5)–O(4)	92.6(4)
C(1)–N(1)–Co	118.2(3)	N(4)–C(6)–C(5)	113.4(5)
O(2)–N(1)–Co	122.9(4)	N(4)–C(6)–C(8)	123.2(5)
O(2)–N(1)–C(2)	155.2(4)	N(4)–C(6)–N(3)	81.7(3)
Co–N(1)–C(2)	81.9(2)	C(5)–C(6)–C(8)	123.4(5)
C(2)–N(2)–O(1)	117.1(5)	C(5)–C(6)–O(3)	145.4(4)
C(2)–N(2)–Co	115.5(4)	C(8)–C(6)–O(3)	90.9(4)
O(1)–N(2)–Co	127.3(4)	C(8)–C(6)–N(3)	155.1(4)
C(5)–N(3)–O(4)	118.1(5)	O(3)–C(6)–N(3)	113.9(3)
C(5)–N(3)–Co	117.8(4)	N(5)–C(9)–C(10)	122.8(5)
O(4)–N(3)–Co	124.0(4)	C(11)–C(10)–C(9)	118.8(5)
O(4)–N(3)–C(6)	154.2(4)	C(10)–C(11)–C(12)	118.8(5)
Co–N(3)–C(6)	81.6(2)	C(13)–C(12)–C(11)	119.6(5)
C(6)–N(4)–O(3)	116.4(4)	N(5)–C(13)–C(12)	122.0(5)
C(6)–N(4)–Co	115.8(4)	(15)–C(14)–Co	117.3(4)
O(3)–N(4)–Co	127.4(3)	C(17–C(16)–Ga	114.6(5)
C(9)–N(5)–C(13)	118.0(5)	C(19B)–C(18)–Ga	121.1(8)
C(9)–N(5)–Co	121.3(3)	C(19A)–C(18)–Ga	109.6(9)
C(13)–N(5)–Co	120.8(4)	C(19B)–C(19A)–C(18)	65(2)
		C(19A)–C(19B)–C(18)	76(2)

composition pathways further steps are difficult to identify. No peak corresponding to a $CoGa_2$ fragment calculated to be at $m/e = 199$ is observed.

No parent molecular ion ($m/e = 542$) is observed in the MS of **2**. A high intensity peak at $m/e = 513$ (100%) corresponds to the initial loss of one ethyl group. Peaks at $m/e = 454$ (10%) and 425 (7%) corroborate further loss of ethyl groups leaving $Ni(dmgGa)_2$. A signal at $m/e = 402$ (4%) might be explained by subsequent elimination of acetonitrile from the glyoximato ligand. As seen above, the fragmentation pattern at this point is increasingly complicated by superposition of various isotope patterns. There is no peak corresponding to $NiGa_2$ ($m/e = 198$).

3.2. *Thermogravimetric analysis*

TGA plots of **1** under 40 mL/min of H_2 or N_2 flow at atmospheric pressure are shown in Fig. 3(a). Under H_2 it reveals four distinctive steps at 88% (170°C), 80% (200°C), 66% (300°C) and 52% (405°C) residual weight. The first step suggests the facile loss of pyridine. The next step corresponds to the removal of two additional ethyl groups. The decomposition continues with the loss of the three remaining ethyl groups in a third step leaving the entity $Co(dmgGa)_2$. The last step is difficult to account for; one possible explanation is the elimination of 2 acetonitrile groups. At 650°C a residual weight of 35% is found, compared to 31% expected for $CoGa_2$. TGA under N_2 also shows 4 decomposition steps, but 55% residual weight appears at 600°C. Apparently decomposition in the absence of hydrogen is a more difficult and incomplete process.

TGA plots of the nickel gallium complex (**2**) under 40 mL/min of H_2 or Ar flow at atmospheric pressure are shown in Fig. 3(b). Under H_2 it reveals two distinctive steps at 78% (200°C) and 42% (330°C) residual weight. The first step suggests the easy loss of the four ethyl groups. The final step is difficult to account for; very tentatively assignment is given to the elimination of four acetonitrile groups. Decomposition continues gradually with increasing temperature and at 500°C the residual weight is 29%, which is less than the value calculated for $NiGa_2$ (36%). The high residual weight (47%) under argon at 500°C indicates that hydrogen is needed for an easier decomposition.

4. MOCVD results and discussion

4.1. *Deposition at 560°C using [(py)(Et)Co(dmg·$GaEt_2$)$_2$] (1)*

Dark, shiny films of CoGa were grown at 2 Torr and 560°C on (100)Si and (100)GaAs using the precursor [Co(Et)(dmg·$GaEt_2$)$_2$·py] (**1**) and hydrogen carrier gas. The SEM micrographs show that the films de-

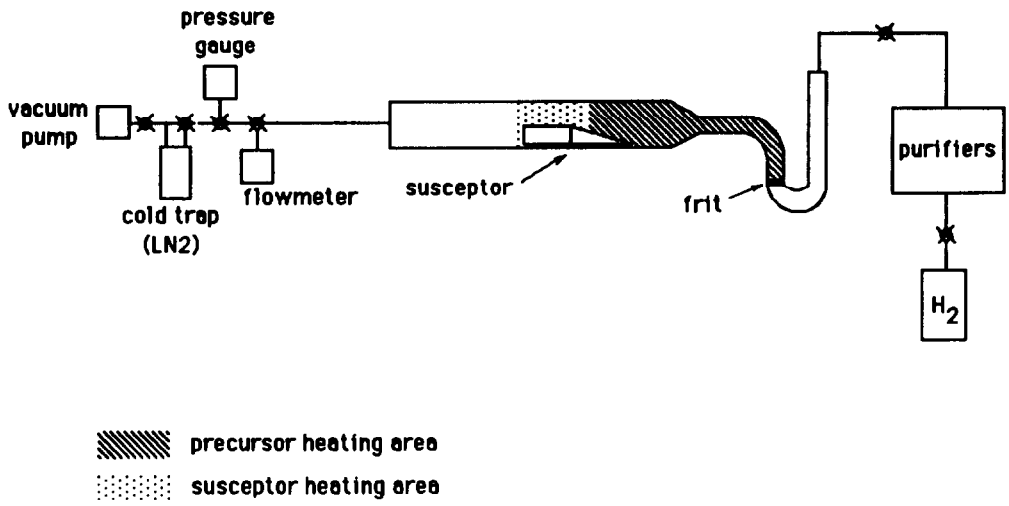

Fig. 2. Quartz tube reactor, inner diameter 2.5 cm and overall length 35 cm.

posited on GaAs(100) and Si(100) consist of plate-like crystallites which are agglomerated to form crystalline nodular grains with a mean size of around 600–900 nm. There is no morphological difference between the samples grown on the two different substrates. Films are inhomogeneous; there are some rough surface areas where the film is relatively thick and smoother areas where the crystallites are sparse on the surface of the substrate, see Fig. 4. Clearly these samples are polycrystalline and there is no preferential orientation.

Composition of the film grown on Si(100) was analyzed by EDS and XPS, see Table 5. EDS analysis gives a Ga:Co ratio of 2.66:1. The error of these values is estimated to be 2%. The film thickness as determined by SEM was found to be 550 nm; this corresponds to a growth rate of 46 nm/min.

Film analysis by XPS after Ar^+ sputtering (4 kV, 20 μamp, 5 min) using an Al Kα X-ray source shows a Ga:Co ratio of 2.42:1. Uncertainty of these values is estimated to be 10%. The carbon contamination is less than 3 atomic percent. The oxygen content is estimated to be 10–20 atomic percent; the overlap of these peaks with Ga Auger peaks does not allow a more accurate determination. There is no evidence for nitrogen contamination. Identification of all the peaks was accomplished by also examining by XPS using the Mg Kα X-ray source see Fig. 5. The Auger peaks are shifted by 233 eV upon shifting the X-ray source and the XPS peaks are unchanged.

Determinination of whether Ga and Co were metallic or bound to oxygen was performed using high resolution spectra to determine the precise binding energy of the Ga 3d, Co 2p and Co 3p levels, see Table 6. Examination of the Co 3p before sputtering shows two contributions: from Co bonded to oxygen (at ~ 61.6 eV) and a metallic Co (~ 59.7 eV). However, only the metallic Co peak is seen after Ar^+ sputtering. This reveals that the oxygen contained in the films is not bonded to Co atoms. Examination of the Co 2p level confirms that only metallic Co is observed in the films. A peak at ~ 778.6 eV corresponds to the binding energy of Co $2p_{3/2}$ and one at ~ 793.6 eV corresponds to Co $2p_{1/2}$. Cobalt oxide peaks at ~ 780.5 eV and ~ 787 eV corresponding to Co $2p_{3/2}$ and a shake-up

TABLE 4. Experimental deposition conditions

Film No.	Precursor	Substrate	Substrate temp.	Pressure	Precursor temp.	Carrier gas	Flow rate (sccm)	Deposition time
1	$[(py)(Et)Co(dmg \cdot GaEt_2)_2]$	(100) GaAs	560°C	2 Torr	65°C	H_2	60	12 h
2	$[(py)(Et)Co(dmg \cdot GaEt_2)_2]$	(100) Si	560°C	2 Torr	65°C	H_2	60	12 h
3	$[(py)(Et)Co(dmg \cdot GaEt_2)_2]$	(100) GaAs	630°C	2 Torr	70°C	H_2	30	12 h
4	$[Ni(dmg \cdot GaEt_2)_2]$	(100) GaAs	560°C	2 Torr	60°C	H_2	60	5 h
5	$[Ni(dmg \cdot GaEt_2)_2]$	(100) Si	560°C	2 Torr	60°C	H_2	60	5 h

line, respectively, are not observed. The spectra of the Ga 3d levels are examined before and after sputtering and then compared with that of a GaAs standard cleaned by Ar^+ sputtering. Before sputtering, the primary peak at ~ 20.5 eV is for Ga oxides. After sputtering, a peak for metallic Ga is seen at ~ 18.8 eV, as well as the peak for Ga oxides; the ratio of Ga oxide to Ga ~ 2.3 : 1. Since the sputtered film shows only metal-

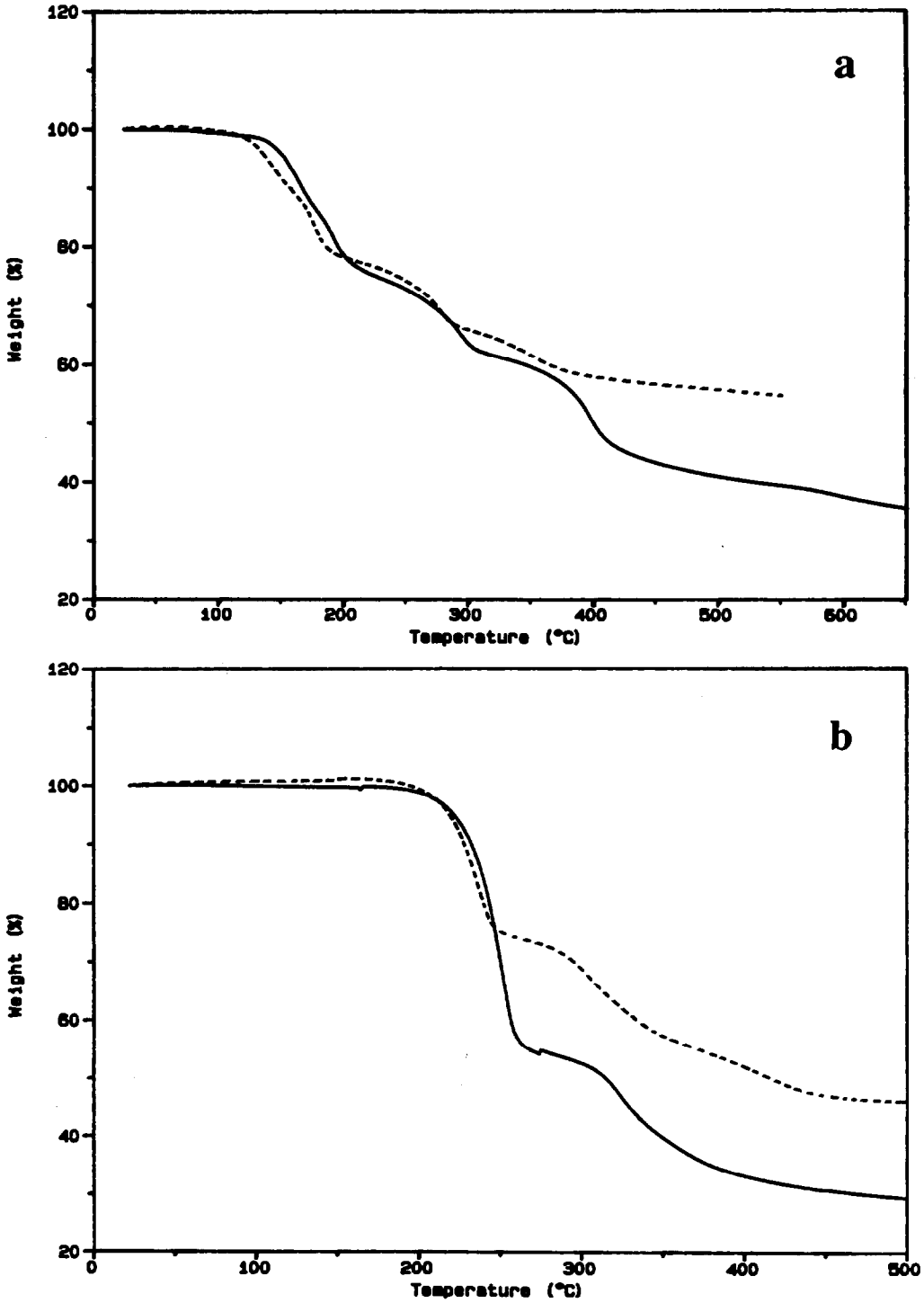

Fig. 3. TGA under a total carrier gas flow rate of 40 cm^3 $min.^{-1}$ (a) [(py)(Et)Co(dmg · $GaEt_2$)$_2$] 1: dashed line under N_2, solid line under H_2. (b) [Ni(dmg · $GaEt_2$)$_2$], 2: dashed line under Ar, solid line under H_2.

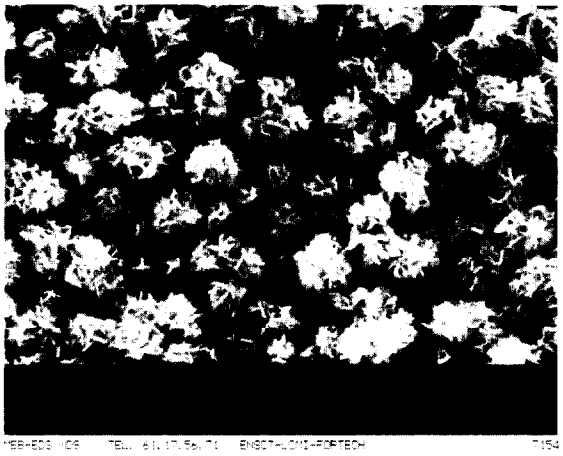

a

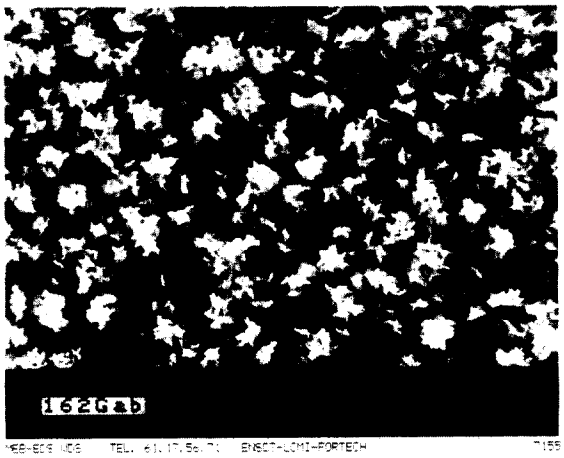

b

Fig. 4. Scanning electron micrographs of β-CoGa (film no. 1, Table 4) at magnification 1.7×10^4. (a) Area of thick deposit. (b) Area of thin deposit.

lic Co but both metallic and oxide Ga, the oxygen in the films can only be bonded to Ga and not to Co.

SIMS analysis of the film on GaAs(100) for depth profiling, Fig. 6(a), shows that the Ga distribution follows the Co distribution. However, distributions on the surface and interface are very diffuse. This can be explained by the heterogeneity and roughness of the sample as previously seen by SEM.

4.2. Deposition at 630°C using [(py)(Et)Co(dmg · $GaEt_2$)$_2$] (1)

Silver-colored films containing small areas of smooth epitaxial β-CoGa films within rough polycrystalline β-CoGa films were grown at 2 Torr and 630°C on (100)GaAs using the precursor [Co(Et)(dmg · $GaEt_2$)$_2$ · py] (1) and hydrogen carrier gas. RHEED analysis of the rough areas of the film gives two typical patterns (no. 1 and no. 2) obtained under different azimuths. These patterns contain the same ring pattern but different spot patterns. The ring patterns correspond to the structure of β-CoGa. Assignment of the d spacing values from ring pattern no. 1 is shown in Table 7. Spot patterns no. 1 and no. 2 are characteristic of (100)GaAs face observed under different azimuths, Fig. 7. RHEED analysis of smooth areas of the film gives a pattern (no. 3) which has the same ring pattern as no. 1 and no. 2, but a different spot pattern. The ring pattern corresponds to the structure of β-CoGa. The spot pattern (Fig. 7) corresponds to a centered cubic structure (CsCl-type) like β-CoGa, not the f.c.c. structure of GaAs (ZnS type). Its assignment reveals a β-CoGa surface oriented (100) which is observed under the azimuth [001]. This clearly indicates that the (100)β-CoGa lattice is matched to the (100)GaAs substrate. These areas of epitaxial growth are embedded in a primarily polycrystalline β-CoGa film.

Scanning electon micrographs, Fig. 8, show crystalline films with numerous holes. These holes have geometric shapes and correspond to etch-pits due to the loss of As from the surface. GaAs thermal degradation begins to occur above 580°C without addition of a partial pressure of As above the surface and is enhanced by the low pressure.

4.3. Deposition at 560°C using [Ni(dmg · $GaEt_2$)$_2$] (2)

Gold-colored polycrystalline films of NiGa were grown at 2 Torr and 560°C on (100)Si and (100)GaAs using the precursor [Ni(dmg · $GaEt_2$)$_2$] (2) and hydrogen carrier gas. Scanning electron micrographs show that the films grown on the two different substrates have the same morphology; their surface is very smooth and uniform. The crystallites observed have a typical size in the range 50–70 nm.

Composition of the film grown on Si(100) was analyzed by EDS and XPS (Table 6). EDS analysis gives a Ga : Co ratio of 2.05 : 1. The error of these values is estimated to be 2%. XPS spectra after sputtering reveals a Ga : Co ratio of 2.83 : 1. Uncertainty of these values is estimated to be 10%. The oxygen contamination is in the 10–20% range; a more accurate value cannot be obtained because of overlaps with Auger peaks. Carbon contamination is determined to be less than 3 atomic percent and careful analysis with XPS and EDS reveals no nitrogen contamination. If there was any nitrogen contamination, Auger peaks would appear at 1105.6 eV and 1123.6 eV using the Al X-ray source. It was shown that none of the peaks in the 1100–1130 eV energy range were Auger peaks. Furthermore, all the XPS peaks were accounted for; the main peak is Ga $2p_{3/2}$ and the minor ones at lower binding energies are characteristic of the X-ray anode. The absence of nitrogen is confirmed by EDS analysis

TABLE 5. Elemental analysis of films

Analysis by EDS						
Precursor	Substrate temperature	Ga : Co ratio	Ga : Ni ratio	% Nitrogen		
[(py)(Et)Co(dmg · $GaEt_2$)$_2$]	560°C	2.66				
[Ni(dmg · $GaEt_2$)$_2$]	560°C		2.05	0%		
Analysis by XPS						
Precursor	Substrate temperature	Ga : Co ratio	Ga : Ni ratio	% Carbon	% Oxygen	% Nitrogen
[(py)(Et)Co(dmg · $GaEt_2$)$_2$]	560°C	2.42		< 3%	10–20%	0%
[Ni(dmg · $GaEt_2$)$_2$]	560°C	0	2.83	< 3%	10–20%	0%

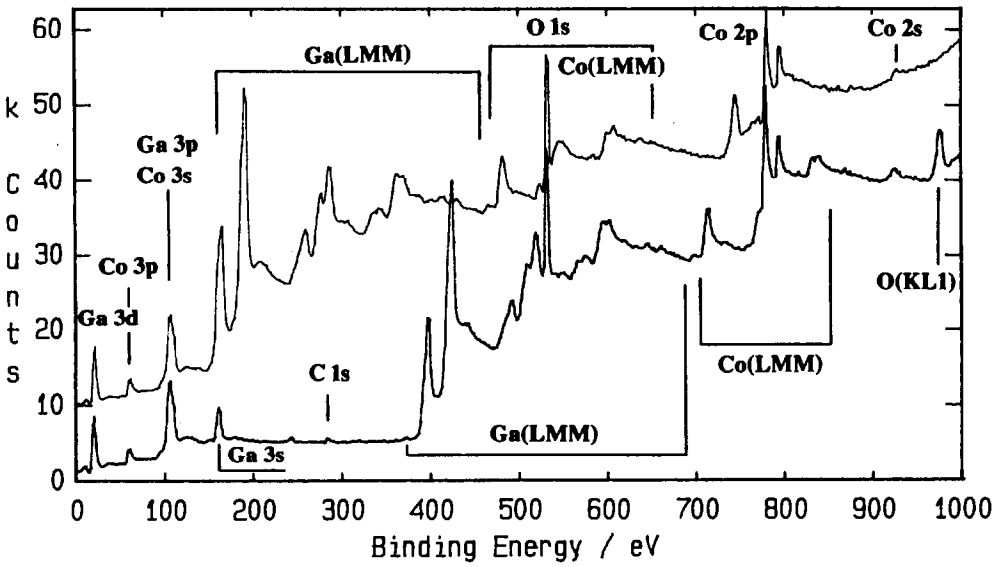

Fig. 5. X-ray photoelectron spectra of β-CoGa (film no. 2, Table 4). Upper trace, Al Kα source. Lower trace, Mg Kα source.

TABLE 6. XPS data

Sample	Ga 3d		Co 3p		Ni $2p_{3/2}$		
	Ga metal (eV)	Ga–O (eV)	Co metal (eV)	Co–O/Co–OH (eV)	Ni metal (eV)	Ni–O (eV)	Ni–OH (eV)
no. 2a	–	20.5	59.7	61.6	–	–	–
no. 2b	18.8	20.5	59.7	–	–	–	–
no. 5a	–	20.7	–	–	853.0	854.2	856.6
no. 5b	18.9	20.5	–	–	853.0	–	–

no. 2a) film no. 2 (Table 4), before Ar^+ sputtering
no. 2b) film no. 2 (Table 4), after Ar^+ sputtering
no. 5a) film no. 5 (Table 4), before Ar^+ sputtering
no. 5b) film no. 5 (Table 4), after Ar^+ sputtering

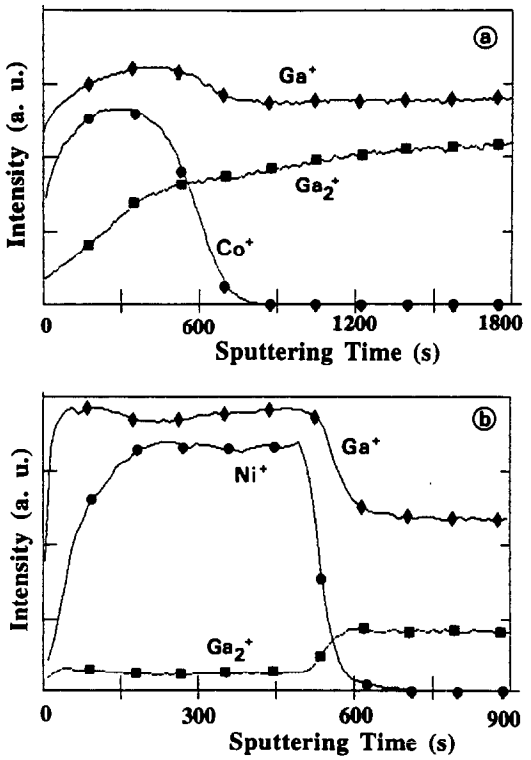

Fig. 6. Secondary ion masss spectrometric traces of (a) β-CoGa (film no. 1, Table 4), and (b) NiGa (film no. 4, Table 4).

of the light elements; there is no nitrogen peak at 0.392 KeV on the spectrum.

Analogous to the CoGa films, determination of whether Ga and Ni were metallic or bound to oxygen was performed using high resolution spectra to determine the precise binding energy of the Ga 3d and Ni 2p levels (Table 6). Examination of the Ni 2p before sputtering shows three contributions: from metallic Ni and Ni bonded to oxygen and OH. However, only the metallic Ni peak is seen after Ar^+ sputtering. This reveals that the oxygen contained in the films is not bonded to Ni atoms. The spectra of the Ga 3d levels are examined before and after sputtering and then compared with that of a GaAs standard cleaned by Ar^+ sputtering. Before sputtering, the primary peak is for Ga oxides. After sputtering, peaks for both metallic Ga and Ga bonded to oxygen are seen. This confirms that the oxygen in the films is only bonded to Ga and not to Ni. A thermodynamic calculation of the system Co, Ga, C, H, O has revealed that Ga_2O_3 is the only oxide which can be formed at low temperatures [12]. The experimental results are in good agreement with this theoretical prediction. Furthermore, the partial oxidation of the sample is possibly enhanced by the fact that O is bonded to Ga in the molecular precursor.

TABLE 7. Assignments of the RHEED ring patterns for β-CoGa (film no. 3, Table 4)

β-CoGa		
Experimental d values (Å)	*hkl*	calculated d values (Å)
–	100	2.88
2.04	110	2.04
–	111	1.66
–	200	1.44
1.23	210	1.29
1.16	211	1.18
1.05	220	1.02
0.99	221	0.96

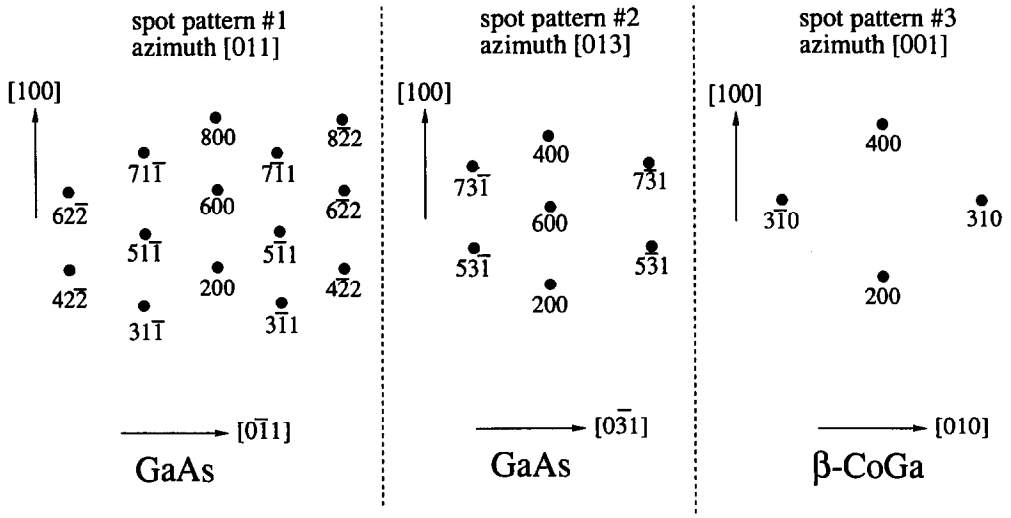

Fig. 7. Assignment of RHEED spot patterns for β-CoGa (film no. 3, Table 4).

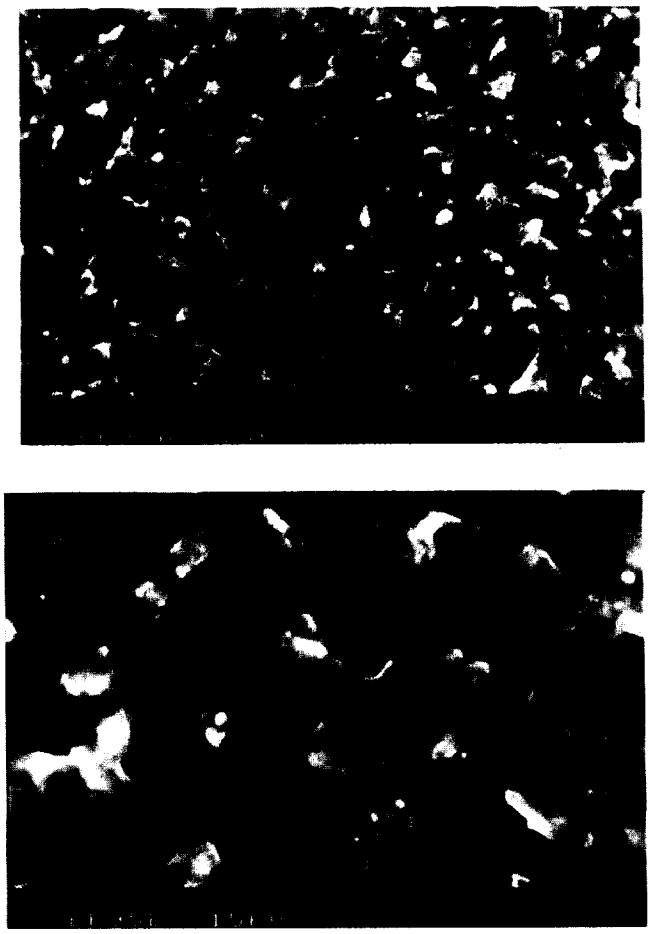

Fig. 8. Scanning electron micrographs of β-CoGa (film no. 3, Table 4) at two magnifications, showing pits due to thermal decomposition of the GaAs surface.

SIMS profiles (Fig. 6(b)) are flat and symmetrical with a relatively sharp interface. Near the surface, there is a Ga excess. This can explain the difference between elemental analysis results from EDS and XPS. Analysis by XPS was probably done on an area near the surface because low energy Ar^+ sputtering was used.

TABLE 8. Assignments of the RHEED ring patterns for film no. 4 (Table 4)

Experimental *d(hkl)* values (Å)	Ni_3Ga_2	NiGa	Ni_3Ga_4	Ni_2Ga_3	$NiGa_4$
2.890	2.854	2.890	2.857	2.865	2.657
1.880	–	–	1.853	1.871	1.882
1.804	–	–	–	1.755	1.797
1.536	–	–	1.556	–	–
1.469	1.423	1.445	1.451	1.481	1.489
1.324	–	–	1.365	1.329	1.331
1.169	1.158	1.180	1.166	1.169	–

Analysis by RHEED shows ring patterns, but no areas with spot patterns. This confirms SEM observations that the sample is only polycrystalline. Epitaxial growth is not observed. Assignment of the RHEED pattern (film no. 4, Table no. 4) is given in Table 8. Comparison between experimental *d(hkl)* and literature values suggests that there is a mixture of phases (NiGa, Ni_3Ga_4, Ni_2Ga_3, and $NiGa_4$). No nickel rich films seem to appear.

5. Conclusion

The M:Ga (M = Co or Ni) ratio in the precursor was shown to be close to that of the deposited films. Some degree of stoichiometry control was shown using a single source precursor. The small discrepancy between precursor and film stoichiometry may be explained by the absence of a direct bond between M and Ga in the precursor. The mass spectrometry results suggest that there is more than one decomposition pathway. Although the major pathway seems to allow for M and Ga to form a bond after the precursor decomposes, a secondary pathway suggests that M and Ga fragments are separated before a bond between the two can form. Previously, deposition using a single source precursor, $[(CO)_4CoGaCl_2(THF)]$, with a direct M–Ga bond resulted in β-$Co_{1.0}Ga_{1.0}$ films; the stoichiometry of the precursor was retained in the films. Because $[(CO)_4CoGaCl_2(THF)]$ contains a direct M–Ga bond, dissociation of the ligands results in a M–Ga fragment. However, the complexes [Co(Et)(dmg · $GaEt_2)_2$ · py] and [Ni(dmg · $GaEt_2)_2$] do not have a direct M–Ga bond; therefore, ligand dissociation does not necessarily result in M–Ga formation. XPS data indicates that the oxygen is bonded to Ga but not to M; this is consistent with precursor structure in which oxygen is bonded to Ga, but not to M. This result is also consistent with thermodynamic calculations.

The suitability of this precursor for deposition of epitaxial β-CoGa films on GaAs was also examined. A major drawback is the high temperature (> 650°C) required for complete decomposition of the precursor; the GaAs substrate begins to decompose at 580°C. The low vapor pressure ($\sim 1 \times 10^{-5}$ Torr) and oxygen contamination are also drawbacks. The absence of nitrogen and low carbon contamination should be considered in future precursor design.

6. Supplementary materials available

Tables A, B, and C mentioned above, and Figs. A–I depicting the various listed NMR data and Figure J containing an SEM photograph of NiGa (film no. 4,

Table no. 4) on GaAs substrate, are available upon request from the authors at UCLA.

Acknowledgments

Support for this collaborative work is gratefully acknowledged to the National Science Foundation (Grant CHE-92-08398) at UCLA and the CNRS (Centre National de la Recherche Scientifique) at the Ecole Nationale Supérieure de Chimie, Toulouse. The authors thank M. Caumon (Université P. Sabatier) for the RHEED measurements.

References

1 H.D. Kaesz, R.S. Williams, R.F. Hicks, J.I. Zink, Y. Chen, H. Müller, Z. Xue, D. Xu, D.K. Shuh, and Y.K. Kim, *New J. Chem.*, *14* (1990) 527.
2 F. Maury, *Adv. Mater.*, *3* (1991) 542.
3 T.B. Massalski (ed.), *Binary Alloys Phase Diagrams*, 2nd ed., ASM International, Vol. 2, 1990, p. 1840.
4 Y. Chen, H.D. Kaesz, Y.K. Kim, H. Müller, R.S. Williams and Z. Xue, *Appl. Phys. Lett.*, *55* (1989) 2760.
5 F. Maury, L. Brandt and H.D. Kaesz, *J. Organomet. Chem.*, *449* (1993) 159.
6 F. Maury, A.A. Talin, H.D. Kaesz and R.S. Williams, *Chem. Mater.*, *5* (1993) 84.
7 U. Kohler, H.D. Hausen and J. Weidlein, *J. Organomet. Chem.*, *272* (1984)337.
8 G. Stringfellow, *Organometallic Vapor-Phase Epitaxy: Theory and Practice*, Academic Press, Inc., San Diego, 1989.
9 G.N. Schrauzer, in W.L. Jolly (ed.), *Inorganic Syntheses*, Vol. 11, McGraw-Hill, Inc., 1968, p. 61.
10 R.J. Meyer, *Gmelins Handbuch der Anorganischen Chemie*, Vol. 57, Verlag Chemie Weinheim, 1969, p. 843.
11 All calculations were performed on VAX 3100 cluster of computers (Department of Chemistry and Biochemistry, University of California, Los Angeles). The programs used in this work included modified versions of the following programs: REDUCE (Broach, Coppens, Becker, and Blessing), peak profile analysis, Lorentz and polarization corrections; SHELXS-86 (G.M. Sheldrick), package of programs, including direct methods, Patterson methods and peak search; ORFLS (Busing, Martin, and Levy), structure factor calculation and full matrix least-squares refinement; ORFFE (Busing, Edwards, and Hamilton), distance, angle and error calculation; HYDROGEN (Trueblood), calculation of hydrogen atomic position; ORTEP (Johnson) figure plotting; PUBLIST (Hoel) structure factor listing. Scattering factors and corrections for anomalous dispersion components from *International Tables for X-Ray Crystallography*, Vol. 4, Kynoch Press, Birmingham, England, 1974.
12 F. Maury *et al.*, to be published.